ROBOMECH Journal

RESEARCH ARTICLE

Open Access

Microfluidic device for rapid investigation of the deformability of leukocytes in whole blood samples

Anas Mohd Noor[1], Taisuke Masuda[2*] and Fumihito Arai[2,3]

Abstract

The mechanical properties of cells, such as leukocytes, in a diseased state differ from those of healthy cells, typically due to their microstructure. The deformability of the cells through a constrictive area is analyzed by the applied stress to the cell. This study investigates the relationship between the sample flow speed and distribution of captured leukocytes based on the cell deformability using a microfluidic device. The device comprises of microfilters that serve as the filtration mechanism. The microfilter gap size gradually decreases from 15 to 3 μm to facilitate the deformability-based separation. Leukocytes have various sizes; hence, they can be separated by microfilters directly from whole blood samples without any cell clogging, and they do not require sample pre-processing such as centrifugation or red blood cell lysis. The distribution of leukocytes captured by the microfilters with respect to the sample flow speed can be analyzed; at higher sample flow speeds of 6 μL/min, small leukocytes with a size of 7 μm could not be captured and they passed through the smallest microfilter gap size of 3 μm. For smaller leukocytes, such as lymphocytes, the distributions are mainly at gap sizes of 4 μm to 8 μm, with most of the lymphocytes captured at the 6 μm microfilter gap size. We conclude that the distribution of the cells captured during the filtration varies depending on the microfilter gap sizes, applied sample flow speed, cell sizes, and the ability of the cells to deform. The deformability imaging profiles of the sample could be developed from the images of the cell distribution, which might be useful for preliminary screening in the clinical applications. This work presents the development of a simple device for the study of cell deformability as the results provide a biophysical marker in high throughput and bulk sample analyses.

Keywords: Microfluidic device, Gradual size decrease microfilters, Leukocyte separation, T and B lymphocytes separation, Cell deformability

Introduction

The mechanical properties and elastic models of cells, such as leukocytes, were first studied nearly four decades ago. These cells have the ability to deform and change their shapes when passing through a very small area, although the cell sizes are more significant than the area sizes [1]. Previous studies have found that the deformability of the leukocytes changes due to disease-related conditions, and they become more stiff (i.e., they are less deformable in patients suffering from diseases such as sepsis-induced disseminated intravascular coagulopathy [2], leukemia (chronic lymphocytic leukemia and acute lymphocytic leukemia) [3], diabetes mellitus [4], Epstein–Barr virus, and acute lung injury [5]). A number of studies have reported that diseases such as cancer (particularly lung and breast cancers) affect the deformability of cells (metastatic cells, in particular) depending on the stage of the tumor [6, 7]. Furthermore, the deformability of the cells also affects their morphological and morphometrical properties (relating to cell diameter and height) as well as elastic properties (Young's modulus) [4, 5]. These changes might be due to the altered cytoskeletal filament network (e.g., actin, microtubules, or lamins)

*Correspondence: masuda@mech.nagoya-u.ac.jp
[2] Institute of Innovation for Future Society, Nagoya University, Nagoya, Japan
Full list of author information is available at the end of the article

organization of the cells [8, 9]. By understanding these properties, essential information may be obtained for further cell rheology studies crucial to understanding disease and improving health. Additionally, the mechanical properties of the cells, such as elasticity, shear characteristics, compression, and deformability, reflect their states and functions and may be used as biophysical markers for the detection of pathological cell changes [2]. Therefore, the analysis of the cell mechanical properties related to disease and drug treatments has attracted much attention [10–12].

Numerous techniques have been used to examine the biophysical properties of cells, particularly cell deformability. Examples include atomic force microscopy (AFM) [13, 14], micropipette aspiration (MA) [15, 16], optical tweezers (OTs) [17, 18], deformability cytometry (DC) [19–21], and microfluidic devices [22–25]. Although AFM is popular it causes lateral instability under loads (i.e., cantilevers) in non-adherent cells such as passive human leukocytes [26]. Additionally, a special mold is required to immobilize the cells. This requirement entails a high cost and the process is time-consuming [27]. OTs increase the local temperature due to the use of laser power, which might damage the cell structure and change the mechanical properties of the cells being analyzed [28]. Thus, this technique has a disadvantage to assessing the mechanical properties of cells compared with MA, which reduces the potential for cell damage, provides wide-ranging applications of measurements, such as elastic coefficient, viscoelastic coefficient, etc. [29, 30], and offers a more straightforward measurement system. However, despite the advantage and wide-ranging applications of MA, the conventional technique still suffers from low throughput and is unsuitable for time-sensitive analyses that entail changes in the measurements over time [31]. DC could overcome the limitations of low throughput. This technique is based on contact modes, such as constriction channels [32], and non-contact modes such as shear stress and pressure gradients [33]. Despite the advantages of DC, it requires a sophisticated system setup including precision pressure control, a high-speed camera, a complex imaging system, and sample pre-processing. In general, DC is more costly than other techniques, such as microfluidic-based systems, analysis via lab-on-chip (LOC) and microTAS (μ-TAS). Therefore, for clinical applications such as sample pre-analysis (i.e., preliminary screening) of bulk samples, a conventional process might not be suitable. Furthermore, preliminary screening before a detailed analysis reduces the time and cost requirements, and detailed analysis can be performed only if required. Thus, a simple device and technique are required to provide a quick analysis result suitable for a clinical process. Various studies have shown that microfluidic technologies for cell mechanical characterization provides advantages compared with other available techniques [34–37].

Currently, the deformability of cells is determined based on single cell conditions. The single-cell analysis method provides high accuracy and reliable results compared with that of a bulk sample, where the measurement of the latter depends on the average value [38]. Although single-cell analysis provides precise information, the measurement system requires a complicated microfluidic structure design and sophisticated peripheral systems. Moreover, these cell characterizations or measurement methods are not suitable for practical clinical applications as they are tedious and suffer from low throughput. Even though bulk analysis provides the average result, it could serve as a useful pre-analysis result, which reduces the clinical processing time. For instance, atypical preliminary screening results could be investigated in more detail only if necessary. Therefore, preliminary screening could reduce tedious work, expedite the measurement process, and, importantly, be suitable for clinical applications.

This research reports the separation of leukocytes directly from whole blood and investigates the distribution of the captured cells using decreasing gap size microfilters on a microfluidic device. Fluorescence-labeled antibodies, such as CD45 antigen (leukocyte common antigen, $CD45^+$ cells mean CD45 positive cells), allow for the identification of leukocytes from the whole blood sample. In our previous work, we developed a clogging-free microfluidic device for separating and counting cells (T and B lymphocytes) on a chip [39]. Our device showed good correlation to fluorescence-activated cell sorting, which is used for counting cells. Therefore, we apply the same concept of cell separation for $CD45^+$ cells in terms of cell deformability. The clog-free microfluidic device consists of multiple sieve filtrations, wherein the microfilter gap size is gradually narrowed. The microfiltration is used to separate the leukocytes in a whole blood sample and allows other cells (red blood cells (RBCs), thrombocytes or platelets) to pass through the filters. The distribution of separated leukocytes corresponding to the microfilter gap sizes and sample flow speed were analyzed. We showed that small leukocytes, namely, of an estimated cell size of 7 μm, could pass through the microfilters even though the smallest gap size was 3 μm when the sample flow speed was increased. We also showed that captured cell distribution images on the microfluidic device could be used as imaging (deformability) profiles. Thus, our method can be realized as a preliminary screening based on cell deformability for bulk samples before more detailed analysis is required. This work contributes to potential applications involving

cell deformability as a biophysical marker for in situ bulk sample analysis with high throughput, which might be useful in drug delivery and disease-related studies.

Materials and methods

Microfluidic device

The microfluidic device consists of polydimethylsiloxane (PDMS) and a glass plate (Fig. 1). The PDMS part was fabricated using a standard soft lithography process. The fabrication process is similar to that used in our previous work (Fig. 2) [39]. Firstly, a photomask was made using a direct write laser lithography (DWL66FS, Heidelberg Instruments Mikrotechnik GmbH, Heidelberg, Germany). Next, a high-contrast epoxy-based photoresist (SU-8 3025, Microchem, Corp., Newton, MA) was spin-coated to a thickness of 40 µm on a 525-µm thick Si wafer (2000 rpm, 30 s). The Si wafer was soft-baked for 40 min at 75 °C. The spin-coated wafer was exposed using a mask aligner (MA-6, SUSS MicroTec AG, Garching, Germany) for 35 s. The post-exposure bake was at 65 and 95 °C for 1 and 5 min, respectively. The Si wafer was developed and dry-etched by a deep reactive ion etching system (D-RIE, RIE-800, Samco, Kyoto, Japan). Octafluorocyclobutane (C4F8) was used for the passivation of the Si mold to create a non-adhesive surface during the PDMS demolding process. The PDMS microfluidic device was prepared using a PDMS pre-polymer (Silpot 184, Dow Corning Toray Co., Ltd., Tokyo, Japan) mixed at a 10:1 (w/w) ratio with a curing agent. The PDMS was poured into the Si mold and baked at 75 °C for 1 h. The cured PDMS was demolded and treated with O_2 plasma (Cute-MPR, FemtoScience, Seoul, South Korea) to facilitate the PDMS surface modification for the glass bonding process.

The microfluidic device comprises two sections: the first section separates the targeted cells from the whole blood sample as a separation area, and the second section collects the remains of the processed sample as a waste area (Fig. 1). The width and length of the separation area are 10 mm and 20 mm, respectively. The separation area comprises micropillar arrays with 12 different groups [39]. Main difference between these pillar arrays is the spacing between each pillar, which we call gap size. The gap size for these 12 micropillar arrays are gradually decreasing in size from the inlet port to the outlet port, 15 µm to 3 µm respectively. The design details of the microfilter are outlined in reference [39]. Larger microfilter gap sizes (e.g., 10 µm and greater) are designed to capture larger $CD45^+$ cells, including neutrophils, basophils, eosinophils, and monocytes, with sizes ranging from 10 to 35 µm. Smaller cells, such as lymphocytes, are more suitably captured by smaller gap sizes. Unfiltered or uncaptured cells, for example, RBCs and platelets, could pass through the microfiltration, as the deformability of RBCs (e.g., ability to contort, twist, and change shape) can result in cell sizes as small as 3 µm [40]. Our preliminary experiments confirmed that micropillar filtration using a filter gap size of 2 µm caused RBCs clogging in the device. Therefore, we chose 3 µm as the smallest filter size. The escape routes in the microfilter arrays prevent cell clogging and fouling on the device during the

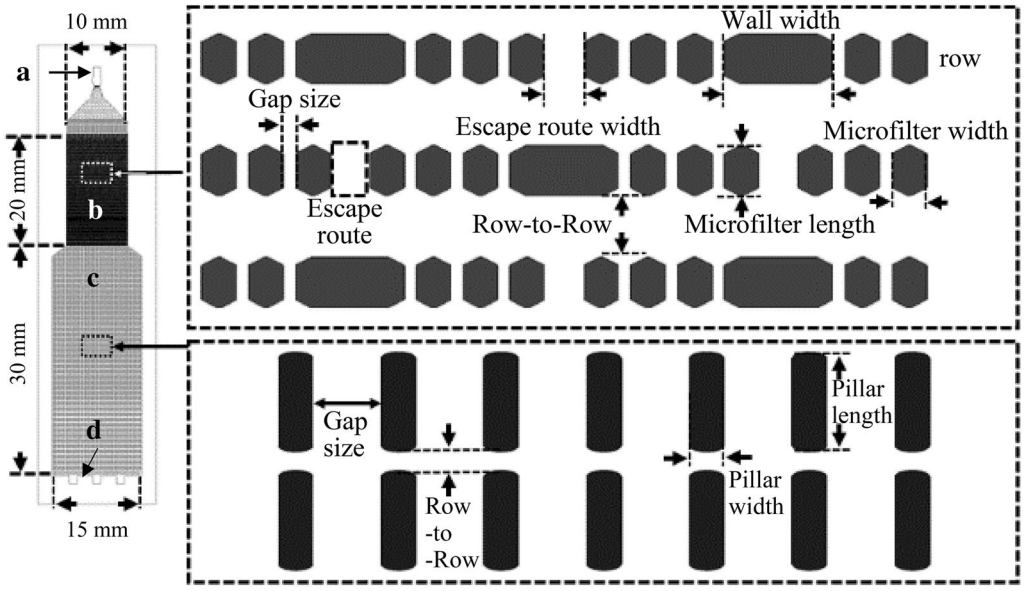

Fig. 1 Schematic diagram of the top view of the microfluidic device. **a** Sample and buffer inlet port. **b** Cell separation area with microfilters of gradually narrowing size. **c** Sample waste area. **d** Air outlets

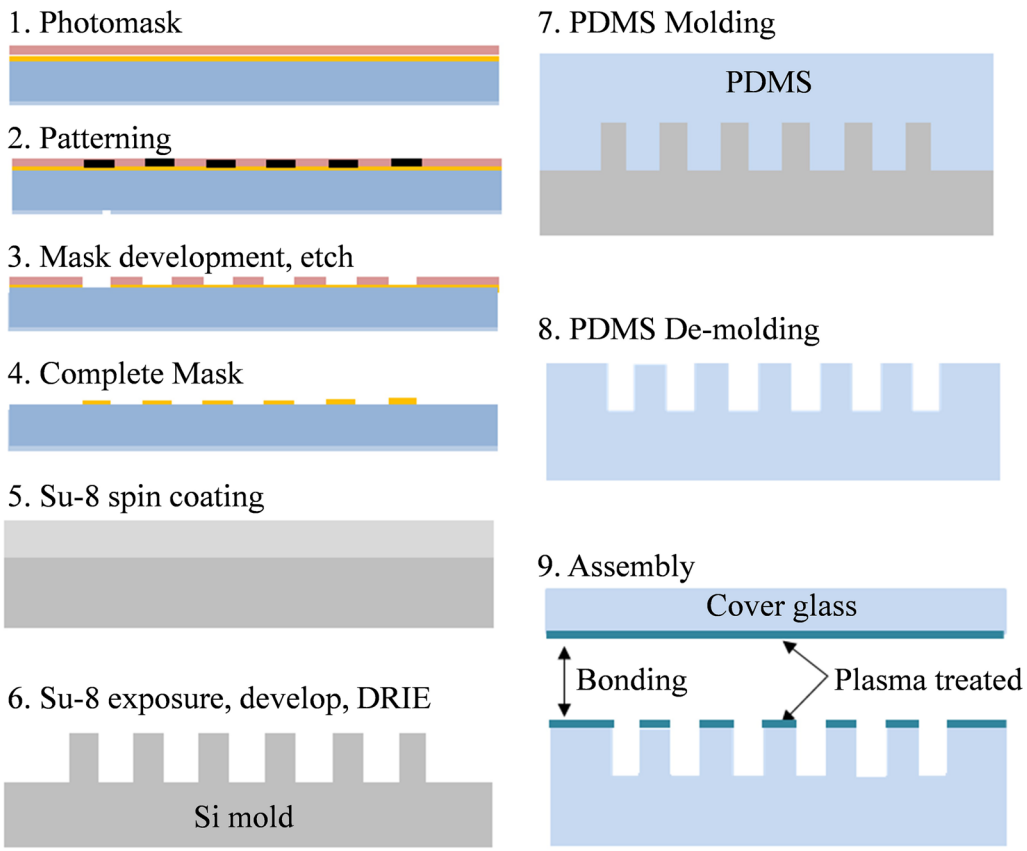

Fig. 2 Fabrication of the microfluidic device using a soft lithography technique

filtration process. The width and length of the waste area are, respectively, 15 mm and 30 mm and contains rectangle pillars for supporting the roof to prevent collapse. The support pillars' width and length sizes are 100 µm and 800 µm, respectively. The gap size and row-to-row of the support pillars are 200 µm and 120 µm, respectively. The height of the microfluidic chip is approximately 40 µm. Thus, the total volume is 8 and 18 µL for the separation and waste area, respectively, and the approximate total volume of this device is 26 µL. Therefore, the sample volume for the device must be less than 18 µL (e.g., 5 to 8 µL) to prevent the sample overflow (i.e., going out) at the outlet. For similar reasons, the waste area was also designed to be larger than the separation area. The waste area design on the microfluidic device will eliminate problems, such as improper sample flushing to the reservoir (e.g., a waste container), that occur when using a conventional microfluidic device. These problems can lead to missing cells and/or cells adhering to the microfluidic tubing wall or container. In addition, sample residue is tedious to process, and processing would involve transferring, which causes cell loss. Therefore, the sample waste collection on-chip design will significantly reduce errors in the cell counting process, particularly for applications that demand precision.

Sample preparation

Human blood samples obtained from healthy donors via venipuncture were placed in 5 mL K2-EDTA vacutainer (BD Vacutainer) tubes. 100 µL of each blood sample was placed in a test tube and gently vortexed at room temperature (24 °C). Then, 20 µL of CD45 antibodies (A07782, CD45-FITC, Beckman Coulter Inc., USA) were added to the test tube and incubated for 15–20 min at room temperature under the protection from light. CD3 and CD19 antibodies (BD Simultest™ CD3/CD19, BD Biosciences, CA, USA) were used for T and B lymphocytes identification. The sample was diluted 10 times with a phosphate-buffered saline dilution buffer (PBS, Sigma-Aldrich, St. Louis, MO, USA) containing 5 mM EDTA (Sigma-Aldrich, St. Louis, MO, USA) and stored in the dark at room temperature prior to performing the experiments. For dynamic observations (e.g., observations of high-speed moving cells), labeling fluorescence antibodies is unsuitable for the observation of uncaptured cells through the microfilters due to the intensity loss under excitation light exposure.

Therefore, we labeled the test sample with the Hoechst 33342 nucleus stain (Thermo Fisher Scientific, MA, USA), which is more robust to the fluorescence emission intensity fading compared with the antibody fluorescence reagent.

Experiment setup and analysis

A prepared blood sample (10 µL) was placed in a tube connected to a syringe pump. The sample flow speeds (i.e., sample flow rates) were set to 1.5, 3, and 6 µL/min, with a total experiment time of 6.7, 3.4, and 1.6 min, respectively. From the preliminary experiments, the sample speed of 1 µL/min indicated that the majority of the blood cells stagnated near the inlet port and were not properly filtered through the microfilters (data is not shown). The clogging of the cells at the inlet port connecting to the sample tube was caused by the high pressure in the microfluidic device, preventing the blood cells from moving towards the microfilters. Therefore, the minimum sample flow speed suitable for this device have decided on 1.5 µL/min.

The prepared sample flowed according to the set sample flow speed and stopped after the entire sample had finished (10 µL of sample). The sheath supply, which moved at a similar speed as the sample, flowed for approximately 10 s longer than the sample supply to prevent inappropriate sample flow to the microfilters. If the sheath supply was not included, dumping of cells near the inlet would occur after the sample has been stopped. After the sheath flow process is completed, the system begins imaging the capture area and determining the count of the captured and uncaptured cells.

The leukocytes count was determined from the sum of the captured and uncaptured leukocytes in the separation and waste areas of the microfluidic device, respectively. Their leukocytes were determined using a custom-made imaging system for automatic cell detection and counting [39]. The leukocyte capture rate in the microfluidic device was defined as:

$$\text{Cell capture rate } (\%) = \left(\frac{\text{Total number of captured cells in the separation area}}{\text{Total number of captured cells in the conbined sepataion and waste area}} \right) \times 100 \quad (1)$$

where the number of captured cells was determined from the separation area and the number of uncaptured cells determined from the waste area.

The captured cell distribution on a specific microfilter gap size could be determined from the total number of captured cells (according to the gap size) over the total number of cells captured at the separation area, defined as:

$$\text{Cell distribution } \left(\text{at specified gap size}\right)(\%) = \left(\frac{\text{Total number of captured cells at specified gap size}}{\text{Total number of captured cells at separation area}} \right) \times 100 \quad (2)$$

The leukocytes were identified using the CD45 antibodies and blue fluorescence by light-emitting diode excitation (M490L4, Thorlabs, USA) and ultraviolet light (M365L2, Thorlabs Inc., NJ, USA), respectively, on a custom inverted fluorescence microscopy and optical system (IDEX Health & Science, LLC, Semrock, NY, USA). Images of leukocytes ($CD45^+$ cells) and T and B lymphocytes ($CD3^+$ and $CD19^+$ cells) were captured and recorded using a high-sensitivity and low-noise CMOS (Complementary metal-oxide-semiconductor) camera (ASI178MC Zhen Wang Optical Company, China, 3096×2080, pixel size 2.4 µm) (Fig. 3).

Results and discussion

Images of cells captured by the microfluidic device are shown in Fig. 4. Clogging and fouling were not observed when using 10 µL of each prepared blood sample for all applied flow speeds. We observed and confirmed that there was no unprocessed (e.g., cell sedimentation) sample at the sample inlet area, which is critical to ensuring that the sample was appropriately processed. The required processing times (i.e., the total time to complete cell separation) were approximately 6.6, 2.8, and 1.6 min at sample flow speeds of 1.5, 3, and 6 µL/min, respectively. Using the developed system (Fig. 3), the $CD45^+$ cells were detected clearly under florescence imaging (Fig. 4), and the captured cells were accurately counted using a simple system.

The $CD45^+$ cells were captured and distributed across the microfilters (Fig. 5). All of the images were taken at the same position in the microfluidic device. The results obtained from the experiments are summarized in Table 1. Table 1 shows the average calculations using the proposed method described in Eq. (2). The distribution and positions of the captured cells in the microfilters demonstrate significant variations depending on the sample flow speed. Using the highest sample flow speed of 6 µL/min as an example, most of the cells were captured at the smaller microfilter gap sizes of 3, 4, and 5 µm; however, for the slowest sample flow speed of 1.5 µL/min, the majority of the cells were captured at gap sizes of 6 µm and greater. The cell counts were averaged for the larger gap sizes of 10–15 µm, as no significant differences in the distribution of the cells were observed by the sample flow speeds. The distribution of the cells increased at gap sizes of 3, 4, and 5 µm for the speed of 6 µL/min compared with that at the other speeds. For

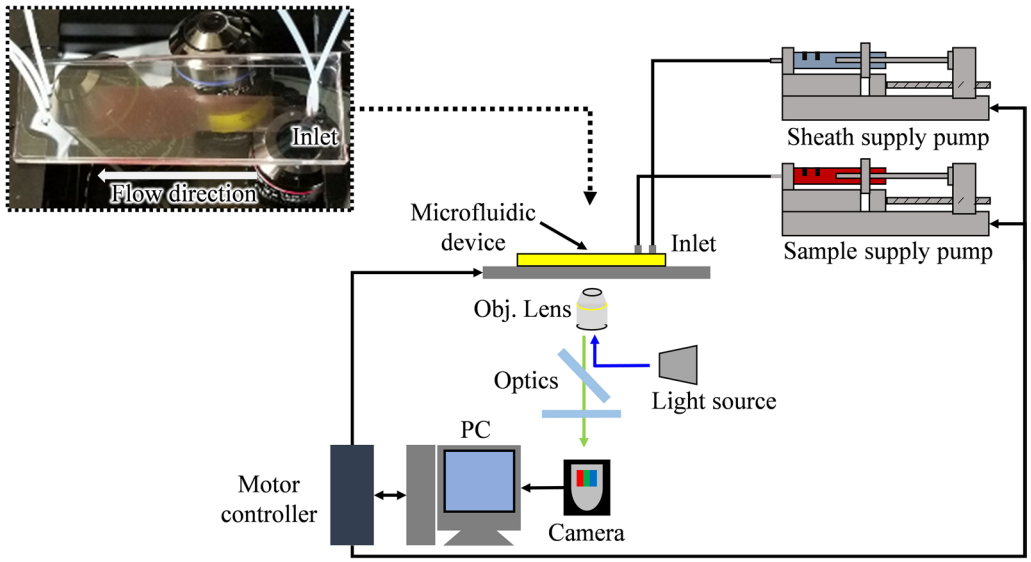

Fig. 3 Schematic of the microfluidic and fluorescence imaging system

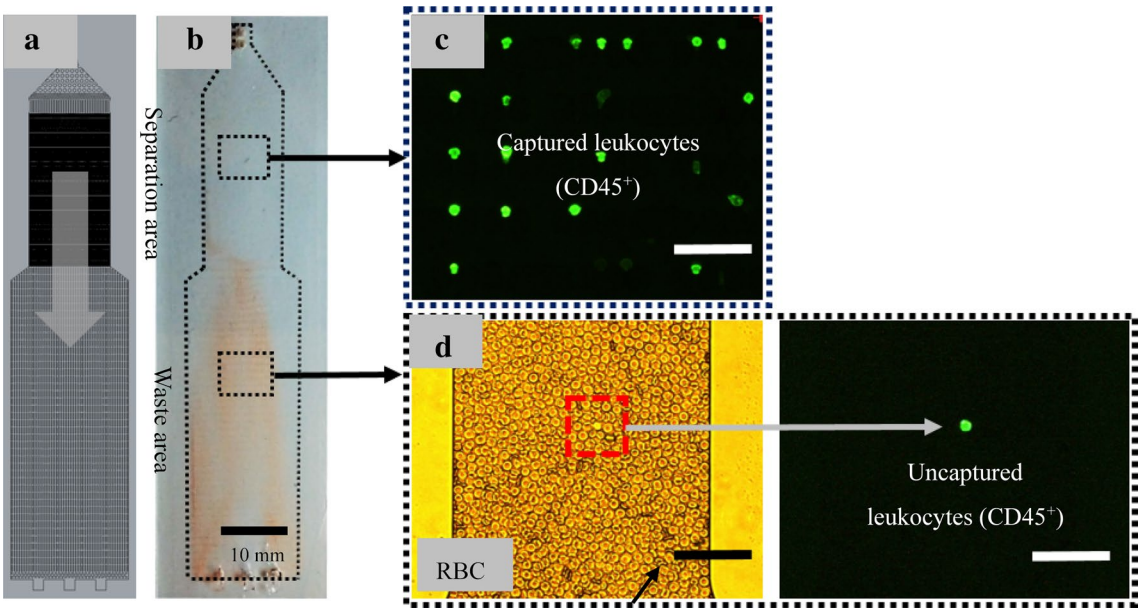

Fig. 4 The separated cells on the microfluidic device. **a** Schematic diagram of the microfluidic device. **b** The fabricated PDMS microfluidic device used for the experiments in this study. The processed blood sample is dumped in the waste area. **c** Captured $CD45^+$ cells (green) in the separation area. No cell clogging was observed in the device. **d** Bright field (left) and fluorescence (right) images of the processed sample in the waste area. Example of an uncaptured $CD45^+$ cell in the waste area identified by fluorescence. The cell size is approximately 7 µm. The lightly shaded area in red in **b** denotes the RBCs that were not captured by the filter and found their way to the waste area instead. Scale bar: 100 µm

instance, at a speed of 1.5 µL/min, the device could capture only 2%, 7%, and 13% of the cells at gap sizes of 3, 4, and 5 µm, respectively. In comparison, at 6 µL/min, the corresponding percentages increased significantly to 12%, 23%, and 13%. The most cells were captured at gap sizes of 9, 6, and 4 µm at speeds of 1.5, 3, and 6 µL/min, respectively.

The cell distribution data clearly indicate that the sample flow speed influenced the positions of the captured

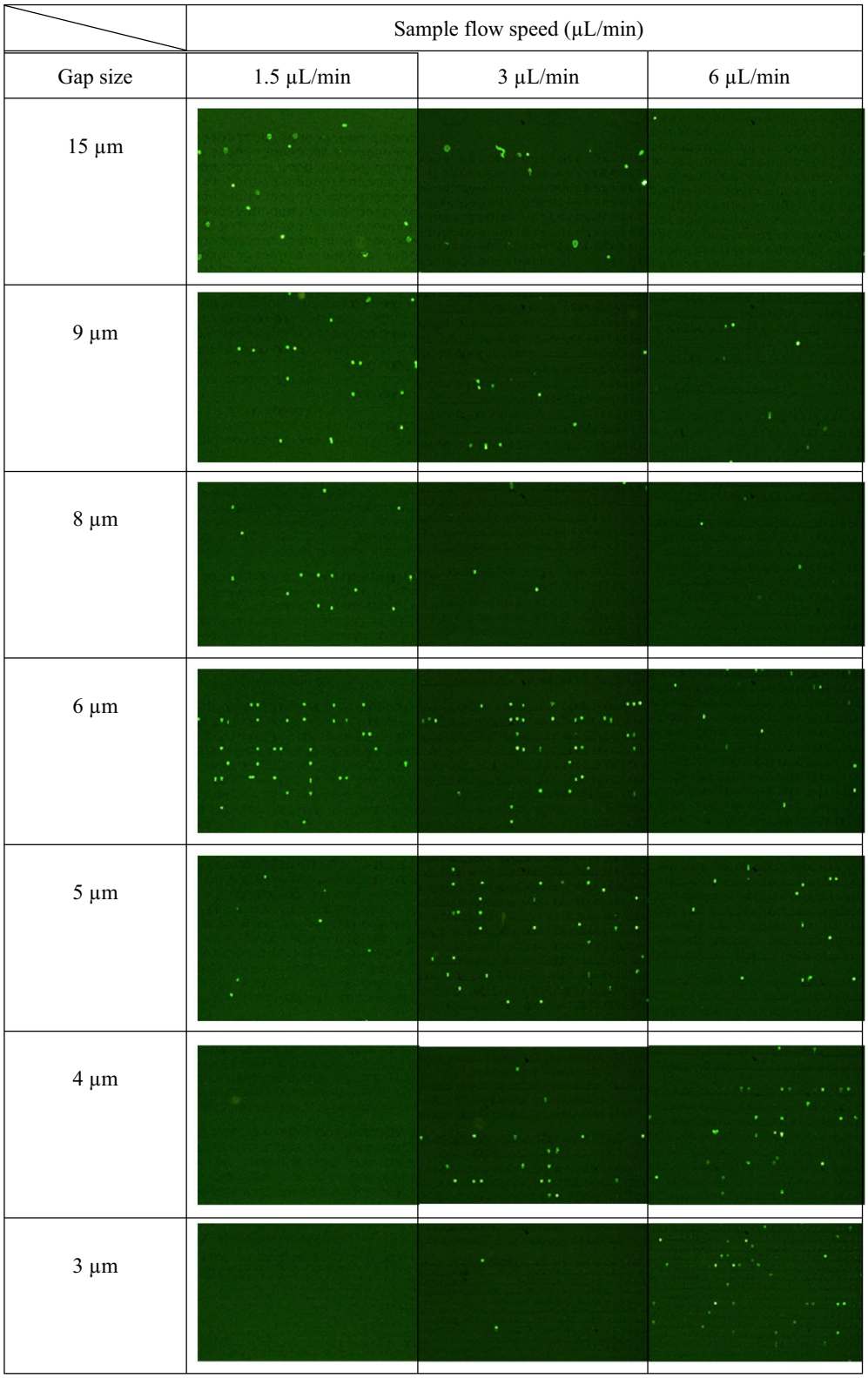

Fig. 5 The distribution of captured cells on the microfilters by sample flow speed and gap size. Images of $CD45^+$ cells (green) are captured at the same position (at the center of the separation area in the microfluidic device). The distribution of the captured cell images can be used as a sample deformability profile

Table 1 Distribution of cells captured at the microfilter gaps at three different flow speeds

	Sample flow speed (μL/min)		
Gap size (μm)	1.5 μL/min	3 μL/min	6 μL/min
10–15	25.5	12.7	8.4
9	26.7	15.8	10.5
8	21.1	19.1	13.0
6	20.0	31.1	17.8
5	3.8	12.8	15.2
4	1.8	7.0	23.4
3	1.1	1.5	11.7

The average cell distribution (%) is shown

cells. These conditions are related to the ability of the cells to deform when pressure (fluid flow) is exerted, which is then used to develop an imaging profile (namely, the sample flow speed changes the cell capture distribution).

The average counts of cells using the microfluidic device are shown in Fig. 6. Using Eq. (1), the performance of the cell capture by the microfluidic device was 100%, 99.7%, and 96% at respective sample flow speeds of 1.5, 3, and 6 μL/min. For the uncaptured cell count, a significant cell loss was observed for the sample flow speed of 6 μL/min compared with the other speeds. Thus, the most efficient speed of this device was 3 μL/min among the three conditions, which required a sample processing time of less than 4 min for 10 μL of prepared sample.

At the highest sample flow speed of 6 μL/min, the hydrodynamic force in the device is large, and, thus, some leukocytes escaped through the smallest micropillar gap size of 3 μm (Fig. 7), which reduced the efficiency of the cell capture rate. This phenomenon could be attributed to the lower stiffness (high deformability) of cells passing through the filter due to the increase in sample flow speed. In addition, the escaped cells, which measure approximately 7 μm, are considered to be small lymphocytes (Fig. 8). Lymphocytes usually range from 7 to 12 μm in size and have been identified as the smallest types of all leukocytes. Moreover, Downey et al. [41] demonstrated that the average size of small lymphocytes is approximately 6 μm, which is smaller than typical RBCs. Thus, some small leukocytes, such as lymphocytes, have a high possibility of escaping the microfilters compared with other cells. However, we did not analyze the phenotypes of the escaped cells, namely, whether they were polymorphonuclear (e.g., neutrophils, eosinophils, and basophils) or morphonuclear (e.g., lymphocytes and monocytes).

Cells that are captured by the microfilters depend on their size, the sample flow speed used, and the gap size of the filters. Leukocytes, including neutrophils, are the most abundant cells (68%), followed by lymphocytes (~20%), and then other cells (e.g., monocyte (<7%), eosinophil (<4%), basophil (<1%) [42]. Therefore, we investigated the distribution of the majority of the lymphocytes (T and B lymphocytes) using a typical sample flow speed (i.e., 3 μL/min) and compared the results (lymphocytes captured distribution) to the majority of leukocytes (neutrophils). As a result, the distribution of these lymphocytes suggested that larger gap size microfilters (e.g., 10–15 μm) had a lymphocyte capture rate 2% lower than the total captured lymphocytes on the microfluidic device. Thus, this suggests that the results in Table 1, for gap sizes ranging from 10 to 15 μm, contain less than 2% of the lymphocytes. Therefore, these larger gap sizes (e.g., 10–15 μm) captured cells other than the lymphocytes, where the majority of the cells are neutrophils.

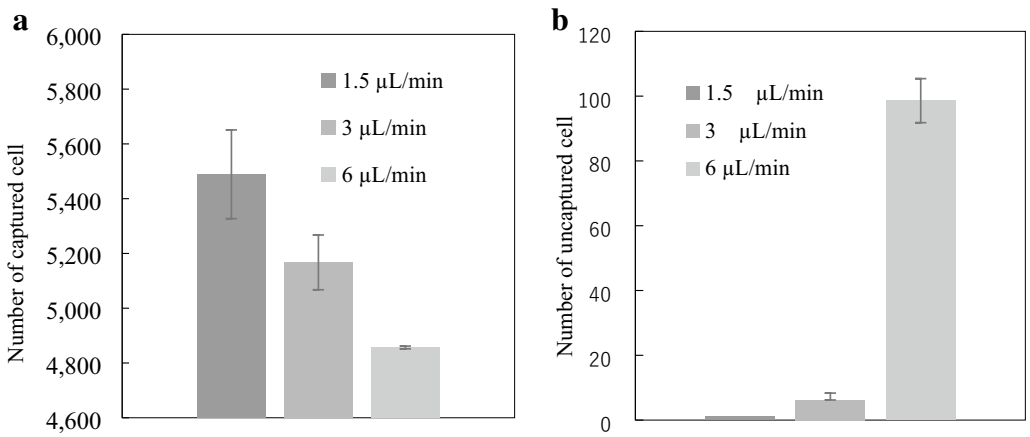

Fig. 6 The average cell count using the microfluidic device. **a** Average captured cell count in the separation area using 1 μL of the whole blood sample. **b** Average uncaptured cell count in the waste area. The error bars denote the standard deviations

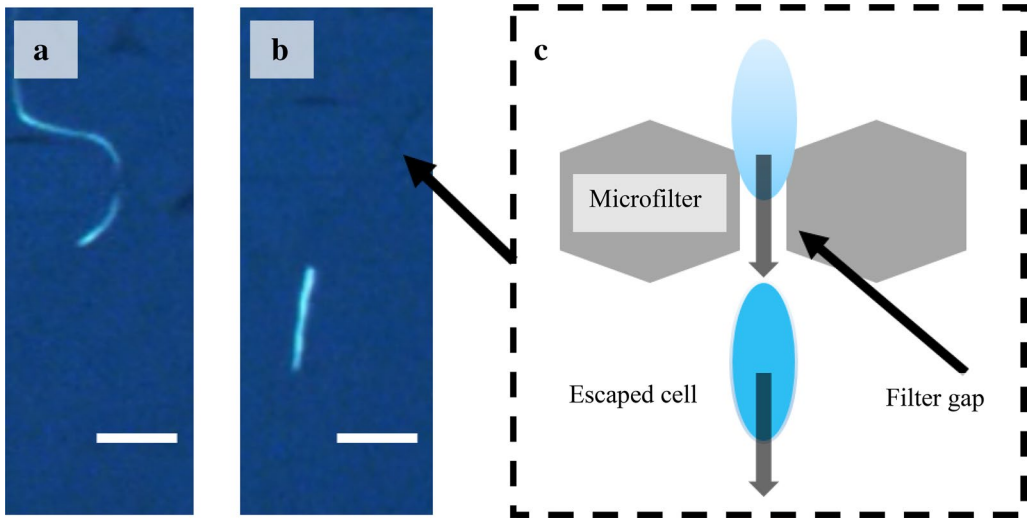

Fig. 7 Images of leukocyte passing through the filter gap. **a**, **b** Images captured during a sample flow speed of 6 µL/min (Exposure time: 100 ms). Leukocytes were stained with Hoechst 33342 (blue). In case of an uncaptured cell, leukocytes enter the microfilters, pass through the filter gap without being captured, and finally reached to the waste area. Scale bar: 20 µm. **c** Illustration of a leukocyte passing through the filter gap

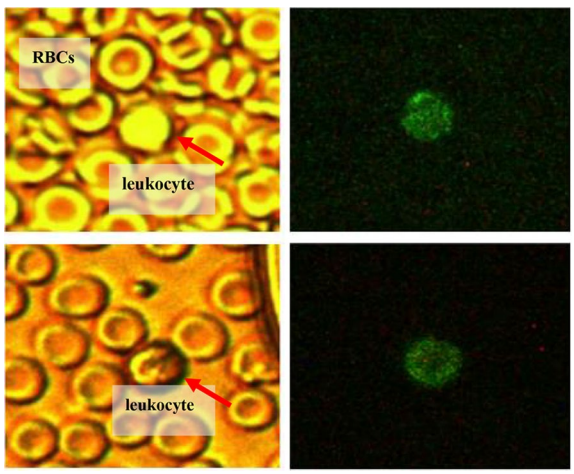

Fig. 8 Examples of escaped cells under a bright field and fluorescence Images. The escaped cells are nearly similar to RBCs in terms of size. The size of an RBC is estimated as 7–8 µm

As shown in Fig. 9, the highest capture of the T and B lymphocytes are at the 6 µm gap size, where the average of the captured cells is about 42% for all test samples. Overall, these results indicate that the higher captured lymphocytes will be mostly at the 4–8 µm gap sizes, where the total captured cell average is about 89%. These results on T and B lymphocytes are similar to those of previous researchers, where lymphocytes were mostly filtered at 6 µm filter sizes [25]. This demonstrates that the deformability profile of healthy lymphocytes is fractionated to a specific value. As shown in Fig. 5, if the deformability is different as in disease and drug treatment, the fractionation position of lymphocytes shifts to either. In the future, we will investigate the clinical potential to detect the deformability profile of in vitro samples of lymphocytes or other leukocytes using this mechanism.

Conclusion

The mechanical properties of cells (e.g., leukocytes and cancer cells), such as deformability, reflect their states and functions. This information can be used as a biophysical marker to detect variations in pathological cells or to distinguish cells for routine clinical examinations targeting early disease diagnosis. Numerous studies demonstrate that the variations in the deformability of leukocytes are related to health conditions. In this work, we developed a simple technique for separating $CD45^+$ cells (leukocytes) directly from a whole blood sample to observe their deformability through microfiltration in a microfluidic device. The proposed microfluidic device successfully recovered all of the $CD45^+$ cells in 10 µL of prepared sample depending on the sample flow speed (e.g., 1.5 and 3 µL/min), without requiring sample preprocessing such as the density gradient centrifugation or RBC lysis. We were more effectively able to detect and count the cells using the simple system than a flow cytometer. Currently, this device can process up to 10 µL of a diluted blood sample without any cell clogging or fouling issues. However, the device design, including the cell separation area, could be varied to support a greater sample volume if required. We demonstrated that

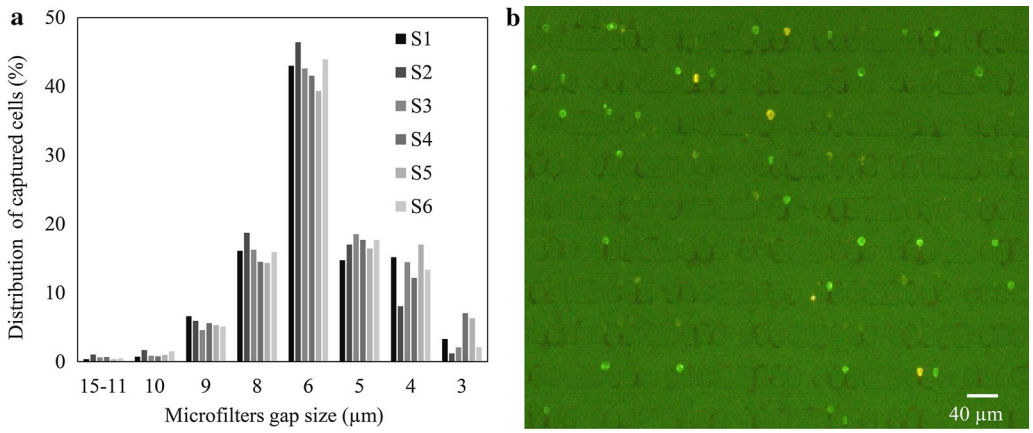

Fig. 9 The Distributions of Captured T and B Lymphocytes. Samples (S) from Individual Donors Flowing at Speeds of 3 μL/min. **a** T and B lymphocytes show higher distribution percentages at a 6 μm gap size and lower distribution percentages at 10–15 μm and 3 μm gap sizes. **b** Example fluorescence image of captured T (green) and B (yellow) lymphocytes at a 6 μm gap size on the microfluidic device

the distribution of the captured cells is influenced by the applied sample flow speed, as some cells were trapped in the microfilters, while some escaped them. We conclude that, if the sample flow speed exceeds 6 μL/min, there is a high possibility that certain leukocytes, such as small lymphocytes, have escaped through the filtration. Moreover, the distribution of the captured cells also depends on the microfiltration gap sizes in which cells are deformed when flowing through the gap. In our experiments, the gap sizes of 9, 6, and 4 μm exhibited the highest percentage of cell captures at sample flow speeds of 1.5, 3, and 6 μL/min, respectively. Furthermore, T and B lymphocytes predominantly captured distributions at gap sizes of 4–8 μm gap, where the 6 μm size showed the highest captured percentages using a typical sample flow speed (3 μL/min). Thus, larger gap sizes (e.g., 9–15 μm) are suitable for capturing other cells such as neutrophils, monocytes, and eosinophils, which are greater than 12 μm in size. Considering that cell deformability reflects its state and characteristics [2], the images of the captured cells in the device (i.e., images of cell distribution) could be used as a deformability profile of the sample. The deformability profile is dependent on the sample flow speed and gap sizes of the microfiltration device. Our future work will include patients with diseases and will compare their cell distributions to those of healthy subjects. By understanding these deformability profile, essential information may be obtained for the cell mechanical properties related to disease and drug treatments. Furthermore, we aim to analyze the cell phenotypes and nuclear shapes in addition to the cell deformability to study the diseased state.

Acknowledgements
Not applicable.

Authors' contributions
AMN and TM performed experiments and analysis. AMN prepared Figs and Tables. AMN, TM and FA contributed to write the manuscript text. AMN, TM and FA designed the study. All authors read and approved the final manuscript.

Funding
This work was supported in part by START Program from Japan Science and Technology Agency, JST., and supported in part by AMED under Grant Number JP19he2202003.

Availability of data and materials
All relevant data are within the paper.

Competing interests
The authors declare that they have no competing interests.

Author details
[1] School of Mechatronic Engineering, Universiti Malaysia Perlis, Arau, Malaysia. [2] Institute of Innovation for Future Society, Nagoya University, Nagoya, Japan. [3] Department of Micro-Nano Mechanical Science and Engineering, Nagoya University, Nagoya, Japan.

Received: 25 November 2019 Accepted: 26 December 2019
Published online: 29 January 2020

References

1. Schmid-Schönbein GW, Sung KL, Tözeren H, Skalak R, Chien S (1981) Passive mechanical properties of human leukocytes. Biophys J 36(1):243–256
2. Morikawa M, Inoue Y, Sumi Y, Kuroda Y, Tanaka H (2015) Leukocyte deformability is a novel biomarker to reflect sepsis-induced disseminated intravascular coagulation. Acute Med Surg 2(1):13–20
3. Zheng Y, Wen J, Nguyen J, Cachia MA, Wang C, Sun Y (2015) Decreased deformability of lymphocytes in chronic lymphocytic leukemia. Sci Rep 5:7613
4. Alexandrova A, Antonova N, Skorkina MY, Shamray E, Cherkashina OV (2017) Evaluation of the elastic properties and topography of leukocytes' surface in patients with type 2 diabetes mellitus using atomic force microscope. Ser Biomech 31(3):16–24
5. Toepfner N, Herold C, Otto O, Rosendahl P, Jacobi A, Kräter M, Ranford-Cartwright L (2018) Detection of human disease conditions by single-cell morpho-rheological phenotyping of blood. Elife 7:e29213
6. Cross SE, Jin YS, Rao J, Gimzewski JK (2007) Nanomechanical analysis of cells from cancer patients. Nat Nanotechnol 2(12):780

7. Plodinec M, Loparic M, Monnier CA, Obermann EC, Zanetti-Dallenbach R, Oertle P, Hyotyla JT, Aebi U, Bentires-Alj M, Lim RY, Schoenenberger CA (2012) The nanomechanical signature of breast cancer. Nat Nanotechnol 7(11):757
8. Lam WA, Rosenbluth MJ, Fletcher DA (2007) Chemotherapy exposure increases leukemia cell stiffness. Blood 109(8):3505–3508
9. Di Cerbo A, Rubino V, Morelli F, Ruggiero G, Landi R, Guidetti G, Alessandrini A (2018) Mechanical phenotyping of K562 cells by the Micropipette Aspiration Technique allows identifying mechanical changes induced by drugs. Sci Rep 8(1):1219
10. Fregin B, Czerwinski F, Biedenweg D, Girardo S, Gross S, Aurich K, Otto O (2019) High-throughput single-cell rheology in complex samples by dynamic real-time deformability cytometry. Nat Commun 10(1):415
11. Zhang X, Chu HK, Zhang Y, Bai G, Wang K, Tan Q, Sun D (2015) Rapid characterization of the biomechanical properties of drug-treated cells in a microfluidic device. J Micromech Microeng 25(10):105004
12. Rotsch C, Radmacher M (2000) Drug-induced changes of cytoskeletal 0structure and mechanics in fibroblasts: an atomic force microscopy study. Biophys J 78(1):520–535
13. Haase K, Pelling AE (2015) Investigating cell mechanics with atomic force microscopy. J R Soc Interface 12(104):20140970
14. Ding Y, Xu GK, Wang GF (2017) On the determination of elastic moduli of cells by AFM based indentation. Sci Rep 7:45575
15. Guo Q, Park S, Ma H (2012) Microfluidic micropipette aspiration for measuring the deformability of single cells. Lab Chip 12(15):2687–2695
16. Esteban-Manzanares G, González-Bermúdez B, Cruces J, De la Fuente M, Li Q, Guinea GV, Plaza GR (2017) Improved measurement of elastic properties of cells by micropipette aspiration and its application to lymphocytes. Ann Biomed Eng 45(5):1375–1385
17. Dao M, Lim CT, Suresh S (2003) Mechanics of the human red blood cell deformed by optical tweezers. J Mech Phys Solids 51(11–12):2259–2280
18. Fraczkowska K, Bacia M, Przybyło M, Drabik D, Kaczorowska A, Rybka J, Wrobel T (2018) Alterations of biomechanics in cancer and normal cells induced by doxorubicin. Biomed Pharmacother 97:1195–1203
19. Gossett DR, Henry TK, Lee SA, Ying Y, Lindgren AG, Yang OO, Di Carlo D (2012) Hydrodynamic stretching of single cells for large population mechanical phenotyping. Proc Natl Acad Sci 109(20):7630–7635
20. Nyberg KD, Hu KH, Kleinman SH, Khismatullin DB, Butte MJ, Rowat AC (2017) Quantitative deformability cytometry: rapid, calibrated measurements of cell mechanical properties. Biophys J 113(7):1574–1584
21. Urbanska M, Rosendahl P, Kraeter M, Guck J (2018) High-throughput single-cell mechanical phenotyping with real-time deformability cytometry, vol 147. Methods in cell biology. Academic Press, Cambridge, pp 175–198
22. Hirose Y, Tadakuma K, Higashimori M, Arai T, Kaneko M, Iitsuka R, Arai F (2010) A new stiffness evaluation toward high speed cell sorter. In 2010 IEEE International Conference on robotics and automation, pp. 4113–4118. IEEE
23. Sakuma S, Kuroda K, Tsai CHD, Fukui W, Arai F, Kaneko M (2014) Red blood cell fatigue evaluation based on the close-encountering point between extensibility and recoverability. Lab Chip 14(6):1135–1141
24. Adamo A, Sharei A, Adamo L, Lee B, Mao S, Jensen KF (2012) Microfluidics-based assessment of cell deformability. Anal Chem 84(15):6438–6443
25. Guo Q, Duffy SP, Matthews K, Islamzada E, Ma H (2017) Deformability based cell sorting using microfluidic ratchets enabling phenotypic separation of leukocytes directly from whole blood. Sci Rep 7(1):6627
26. Rosenbluth MJ, Lam WA, Fletcher DA (2006) Force microscopy of nonadherent cells: a comparison of leukemia cell deformability. Biophys J 90(8):2994–3003
27. Giessibl FJ (2003) Advances in atomic force microscopy. Rev Mod Phys 75(3):949
28. Zhang H, Liu KK (2008) Optical tweezers for single cells. J R Soc Interface 5(24):671–690
29. Yu H, Tay CY et al (2010) Mechanical behavior of human mesenchymal stem cells during adipogenic and osteogenic differentiation. Biochem Biophys Res Commun 393:150–155
30. Sato M, Ohsima N, Nerem RM (1996) Viscoelastic properties of cultured porcine aortic endothelial cells exposed to shear stress. J Biomech 29(4):461–467
31. Lee LM, Liu AP (2014) The application of micropipette aspiration in molecular mechanics of single cells. J Nanotechnol Eng Med 5(4):040902
32. Ren X, Ghassemi P, Babahosseini H, Strobl JS, Agah M (2017) Single-cell mechanical characteristics analyzed by multiconstriction microfluidic channels. ACS Sens 2(2):290–299
33. Otto O, Rosendahl P, Mietke A, Golfier S, Herold C, Klaue D, Wobus M (2015) Real-time deformability cytometry: on-the-fly cell mechanical phenotyping. Nat Methods 12(3):199
34. Xue C, Wang J, Zhao Y, Chen D, Yue W, Chen J (2015) Constriction channel based single-cell mechanical property characterization. Micromachines 6(11):1794–1804
35. Shukla VC, Kuang TR, Senthilvelan A, Higuita-Castro N, Duarte-Sanmiguel S, Ghadiali SN, Gallego-Perez D (2018) Lab-on-a-Chip platforms for biophysical studies of cancer with single-cell resolution. Trends Biotechnol 36(5):549–561
36. Raj A, Sen AK (2018) Microfluidic sensors for mechanophenotyping of biological cells. Environmental chemical and medical sensors. Springer, Singapore, pp 389–408
37. Li YJ, Yang YN, Zhang HJ, Xue CD, Zeng DP, Cao T, Qin KR (2019) A microfluidic micropipette aspiration device to study single-cell mechanics inspired by the principle of wheatstone bridge. Micromachines 10(2):131
38. Myrand-Lapierre ME, Deng X, Ang RR, Matthews K, Santoso AT, Ma H (2015) Multiplexed fluidic plunger mechanism for the measurement of red blood cell deformability. Lab Chip. 15(1):159–167
39. Noor AM, Masuda T, Lei W, Horio K, Miyata Y, Namatame M, Arai F (2018) A microfluidic chip for capturing, imaging and counting $CD3^+$ T-lymphocytes and $CD19^+$ B-lymphocytes from whole blood. Sens Actuators B Chem 276:107–113
40. Sosa JM, Nielsen ND, Vignes SM, Chen TG, Shevkoplyas SS (2014) The relationship between red blood cell deformability metrics and perfusion of an artificial microvascular network. Clin Hemorheol Microcirc. 57(3):275–289
41. Downey GP, Doherty DE, Schwab B 3rd, Elson EL, Henson PM, Worthen GS (1990) Retention of leukocytes in capillaries: role of cell size and deformability. J Appl Physiol 69(5):1767–1778
42. Waite L, Fine JM (2007) Applied biofluid mechanics. McGraw-Hill Publishing Company Inc, New York

Publisher's Note